1984

Limits on Arcsecond-Scale Fluctuations in the Cosmic Microwave Background

James E. Knoke '82
Class of 1982, Haverford College

Bruce Partridge
Haverford College, bpartrid@haverford.edu

M. I. Ratner

I. I. Shapiro

1984

Limits on Arcsecond-Scale Fluctuations in the Cosmic Microwave Background

James E. Knoke '82
Class of 1982, Haverford College

R. Bruce Partridge
Haverford College

M. I. Ratner

I. I. Shapiro

THE ASTROPHYSICAL JOURNAL, 284:479–490, 1984 September 15

LIMITS ON ARCSECOND-SCALE FLUCTUATIONS IN THE COSMIC MICROWAVE BACKGROUND

J. E. KNOKE[1] AND R. B. PARTRIDGE
Haverford College, Haverford, PA

AND

M. I. RATNER AND I. I. SHAPIRO
Harvard-Smithsonian Center for Astrophysics, Cambridge, MA
Received 1983 November 10; accepted 1984 March 29

ABSTRACT

We used the NRAO Very Large Array in its C configuration at a wavelength of 6 cm to set upper limits on the rms fluctuation of sky brightness on angular scales of 6″–18″ from sources too weak to be detected individually. At the highest resolution, we establish a limit of 8 μJy per beam area on the rms sky fluctuation. If this fluctuation level is the result of a Poisson distribution of unresolved sources, each of flux density S_0 Jy, then the number density of such sources per steradian must be less than 0.08 S_0^{-2} sr^{-1}. For alternative models in which all sources are resolved, we derive less stringent limits. Our limits on the rms sky fluctuation also establish limits on the rms temperature fluctuation ΔT for simple models of fluctuations in the cosmic microwave background: $(\Delta T/2.7\ \mathrm{K}) < 3.2 \times 10^{-3}$ and $(\Delta T/2.7\ \mathrm{K}) < 1.2 \times 10^{-3}$ for Gaussian temperature fluctuations of angular scale 6″ and 18″, respectively.

Subject headings: cosmic background radiation — radio sources: extended

I. INTRODUCTION

Observations of fluctuations in the intensity of the cosmic microwave background provide cosmologically important information. If the photons of the microwave background reach us unscattered from the epoch of their decoupling from matter at redshift $z \approx 1000$, then the angular scale and the amplitude of the background fluctuations are related to the mass and amplitude of density perturbations at that early epoch (Silk 1968; Sunyaev and Zel'dovich 1970), and hence can set useful constraints on theories describing the formation of galaxies and other massive bound systems. Even if the photons scattered at a lower redshift, measurements of the angular scale and amplitude of the intensity fluctuations would tell us something about the formation of galaxies and clusters and possibly also about the scattering mechanism itself (see Hogan 1982). Note that in either case, observations of background fluctuations would provide information about the properties and distribution of matter at redshifts much larger than the redshift of the most distant observed quasar.

Searches for fluctuations in the microwave background have been made mostly on angular scales of 5° and above (Melchiorri *et al.* 1981; Fixsen, Cheng, and Wilkinson 1983; Lubin, Epstein, and Smoot 1983), or at $\sim 10'$ (e.g., Parijskij, Petrov, and Cherkov 1977; Partridge 1980; Uson and Wilkinson 1984). A search for fluctuations on smaller angular scales, say $\sim 10''$, is also of interest. First, density inhomogeneities of roughly galactic mass at $z = 1000$ would have an apparent angular diameter $\sim 10''$ (Weinberg 1972, for $H_0 = 50$ km s^{-1} Mpc^{-1} and $q_0 = 0.1$). Second, Hogan (1980, 1982) has presented models in which re-ionization of the intergalactic medium prevents an unimpeded view back to the epoch of decoupling. In these models, larger amplitude fluctuations in the microwave background are expected at smaller angular scales than in conventional models. More generally, in view of the model dependence of the predicted amplitude and angular spectrum of the background fluctuations, it seems prudent to extend observations to all angular scales, including smaller ones. Finally, sensitive searches set limits on the flux density from unresolved discrete sources, and hence have a bearing on the extrapolation of the radio luminosity function to lower values of the flux density.

Observations at centimeter wavelengths on an angular scale of $\sim 10''$ require the use of aperture synthesis. This technique, however, has one major disadvantage over filled-aperture measurements: the lack of sensitivity due primarily to limited bandwidth and higher angular resolution (see § VII). The large number of telescopes in the Very Large Array (VLA) of the NRAO[2] offers increased sensitivity, but not to the level achieved using filled-aperture telescopes. On the other hand, aperture synthesis has some advantages in addition to providing arcminute or better angular resolution. This technique provides a two-dimensional map of the sky, whereas previous filled-aperture observations have provided information only about a one-dimensional "slice" of the sky. Since the geometry of density inhomogeneities may be quite irregular (Zel'dovich 1978), two-dimensional information is desirable.

Here we report results based on 20 hours of observations obtained at the VLA in excellent weather during the nights of 1980 October 1 and 2. Following the basic scheme of Martin, Partridge, and Rood (1980), we first produced synthesis maps of a single field and then analyzed the variance of the fluctuations in those maps. Our final upper bound on the amplitude of small-scale fluctuations of the cosmic background is set not by thermal noise, but by our inability to find and remove data suffering from small instrumental problems which would not be significant for other observing programs. Therefore in §§ III and IV we discuss our editing of the data and our mapping

[1] Now at SofTech, Waltham, MA.

[2] The National Radio Astronomy Observatory is operated by Associated Universities, Inc., under contract with the National Science Foundation.

procedures at more than the usual level of detail. On the other hand, because our observations yield only upper bounds on the fluctuations in the sky brightness, we use simple approximations in obtaining those bounds, as described in §§ V and VI. Finally, in § VII we use these upper bounds to derive corresponding bounds on the parameters of simple numerical models of the fluctuations in the microwave background. These results are presented in Table 4, and discussed in § VIII.

A side benefit of the observations reported here is that they also provide a very sensitive survey of discrete sources. In fact, we detected flux densities down to 75 μJy at the 5 σ level. These results will be discussed in a separate paper (Hilldrup, Partridge, and Ratner 1984).

While this paper was being completed, we received a preprint (Fomalont, Kellermann, and Wall 1984) reporting the results of a similar observing program made at $\lambda = 6$ cm using the VLA in the D configuration, which provides resolution $\gtrsim 18''$. We compare our results with theirs in §§ VI and VIII below.

II. OBSERVATIONS

a) Selection of the Survey Area

We chose to map an area centered on $3^h10^m00^s$ right ascension, 80°08′00″ declination (1950.0 coordinates). The high declination allowed continuous observations for a 12 hour period each night and ensured that the baseline traces in the *u-v* plane (Kraus 1966) were approximately circular, thus yielding more uniform coverage. This particular region of the sky had been surveyed earlier at wavelengths of 3.7 and 11 cm in a preliminary search for fluctuations in the cosmic microwave background (Martin, Partridge, and Rood 1980). In that survey no sources with a flux density above ~3 mJy at 11 cm were found in the area of our present map.

b) Array and Receiver Parameters

We used the VLA in its C configuration, with a maximum baseline spacing of 3.5 km or 5.6×10^4 wavelengths at the central frequency of 4885 MHz. At this frequency the full width at half-maximum power (FWHM) of the primary beam of each telescope is $\theta_P = 9'.06$ (Napier and Rots 1982). We used the maximum available bandwidth, measured by the NRAO staff to be 55 MHz between half-power points. For most of our observations, 24 telescopes were employed. Finally, we averaged the data (fringe visibilities) for 30 s before recording them for later processing.

III. CALIBRATING AND EDITING THE VISIBILITY DATA

Every 20 minutes we interrupted the observations of our map area to observe a calibrator source for four minutes. As our primary flux density calibrator, we used 0212+735 for which we assumed $S = 2.23$ Jy at 4885 MHz, as recommended by the VLA staff (based on observations preceding our own by just a few weeks). A secondary calibrator was 1928+738, for which we determined $S = 3.08$ Jy with a statistical accuracy of ±2% (Hilldrup, Partridge, and Ratner 1984). These observations were used with standard VLA procedures (Hjellming 1982*a*) to calibrate our visibility amplitudes and phases. Since the level of polarization of any fluctuations in the microwave background was expected to be small, we did not execute the procedures required to calibrate observations of linear polarization.

In editing the visibility data, our general philosophy was to eliminate suspect data rather than to retain it. We employed many of the standard VLA procedures (Hjellming 1982*a*, *b*) to locate (and drop) faulty data records, data contaminated by interference, and data affected by abrupt phase changes or by the shadowing of one antenna by another. For example, on about a dozen occasions each night, we found evidence of abrupt phase changes in the signals from one or more of the antennas. Since our survey field was devoid of strong sources, such phase changes could be detected only from calibrator observations. When the relative phase of two successive observations of a calibrator suggested that such a change had occurred at an unknown time in between the two calibrator observations, we dropped *all* intervening data from such antennas. Also, checks of the visibility amplitudes from each correlator revealed some with large values, probably caused by some interference; these visibility data were eliminated. At this point ~70,000 of a total of ~540,000 visibility records had been dropped.

Despite the elimination of these suspect data, there were still some faint "artifacts" visible in the maps obtained from the retained data. The most prominent of these were several faint partial rings concentric with the phase center of the map. It is known that such rings can be caused by a small, constant or nearly constant (complex) bias or offset lasting for at least a few hours in the visibilities from one baseline (cf. Fomalont, Kellermann, and Wall 1984). In the simple case of a constant bias fully sampled over a complete circle about the origin of the *u-v* plane, the resulting map artifact is the Fourier transform of such a circle, namely a Bessel function which appears as a central peak and a set of concentric circular rings which decrease in amplitude with increasing radius (Bracewell 1965). Less idealized *u-v* sampling leads to more complicated artifacts which still exhibit symmetry about the center of the map. In order to eliminate any remaining anomalous visibility amplitudes, as well as any data from noticeably biased or abnormally noisy correlators missed in earlier searches, we scanned summaries of the visibility amplitudes, and of the sine and cosine components separately, for each baseline. This inspection led us to drop ~27,000 more visibility records. In all, we eliminated a total of 18% of the visibility records. Although this elimination removed all "ring" artifacts, it remains possible that a large number of individually undetectable offsets due to biases or cross-talk between antennas are still adding random-looking "noise" preferentially near the map center. We suspect that this instrumental problem sets the practical limit of the sensitivity of our analysis.

IV. CONSTRUCTION OF MAPS

NRAO mapping programs of the AIPS software package (as available in 1982) were used on the MODCOMP and VAX computers in Charlottesville to make maps from each night's data separately, and from the combined data. All maps discussed below were made with $(1024)^2$ square cells each 2″ on a side. We thus mapped a region of the sky approximately 34′ square. The phase center of all maps was chosen to be the astrometric position used to point the antennas, in the usual manner. We constructed maps in total intensity I and in Stokes parameters Q and V.

a) Weighting of the Complex Visibilities

In accord with normal procedure for producing maps from VLA data, each set of complex visibilities was gridded and weighted before the fast Fourier transforms were made to obtain each map. The "exponential-times-sinc" grid convolu-

tion (Greisen 1979) was used, and the corresponding gridding correction was applied to all maps. To maximize sensitivity to weak sources (and extended intensity fluctuations), we gave each grid cell in the u-v plane a weight proportional to the amount of data in that cell. Although this proportional (or "natural") weighting, as opposed to uniform weighting, slightly broadened the synthesized beam, it also lowered the variance of the noise in the maps without significantly changing the level of the sidelobes. The maximum sidelobe response of the synthesized beam was only 1.5% of the peak response. This synthesized beam was well represented down to 15% of peak power by a Gaussian profile with FWHM of 6.″4 in right ascension and 6.″0 in declination. Had we chosen to weight the data uniformly, the corresponding FWHM dimensions of the synthesized beam would have been 5.″4 and 5.″1, respectively.

b) *Subtraction of Discrete Sources*

Despite our attempt to select a region of the sky free from significant discrete radio sources, a few sources and their sidelobes were visible in our maps. To eliminate these from our maps we used the "clean" program (Clark 1980), but only on the center quarter ($[512]^2$ cells) of the map. We departed from the usual procedure by not restoring these "cleaned" sources to the map.

The level to which the maps were "cleaned" was important since we wished to eliminate only discrete sources and not the fluctuations we want to study. Using a gain of 0.3, we removed "clean" components until roughly equal numbers of positive and negative components were being removed. At this point, we assumed we were beginning to remove noise, or fluctuations, rather than detectable sources, from the map. From each of the total intensity maps we removed 100 components, the smallest absolute value of flux density removed being ~ 20 μJy. Of these 100 components, nine were negative, and 84 were clearly associated with one or another of the weak discrete sources in our map. For maps made in Stokes parameters Q and V, in which even the brightest discrete source in the field was barely visible, we removed fewer points: 25, of which 11 were negative. The corresponding smallest flux density level was also ~ 20 μJy.

The root mean square (rms) noise levels of the maps were $\sim 15\frac{1}{2}$, ~ 15, and ~ 16 μJy per synthesized beam area for the Q, V, and I maps, respectively. The close agreement among all three sets suggests that atmospheric and/or instrumental noise dominated the noise introduced by either weak sources or by fluctuations in the microwave background (see §§ V and VII).

c) *Tapered Maps*

In addition to the map described above, we made a series of maps using u-v plane data which had been weighted by a Gaussian taper. The use of taper has the effect of reducing the weight of data from long baselines, and hence of broadening the synthesized beam. In the NRAO mapping programs of the AIPS package the width of a Gaussian taper is specified by D_T, the radius in the u-v plane in thousands of wavelengths ($k\lambda$) at which the taper weighting function is 0.3 times its value at the origin. We made maps with Gaussian tapers ranging from 120 $k\lambda$ (which had negligible effect on the synthesized beamwidth) to 1.2 $k\lambda$ (which broadened the synthesized beam from $\sim 6''$ to $\sim 1.'4$). In § VII we show that for the purpose of providing upper bounds on the level of any fluctuations in the microwave background, these maps are more valuable than the untapered maps.

V. ANALYSIS

We seek to determine the level of fluctuation in our maps due to any anisotropy in the microwave background or to undetected sources in our field. To distinguish between these fluctuations (hereafter called "sky" fluctuations or "sky" noise), and other fluctuations in our maps due to instrumental noise, interference, and atmospheric emissions (hereafter denoted together as "local" noise), we follow Martin, Partridge, and Rood (1980) in computing least-squares estimates of the mean square levels of the two categories of noise. It is possible to estimate the two levels simultaneously because the amplitude of the "sky" fluctuations, if any, would be proportional to the power pattern of the individual antennas of the array, whereas the "local" noise is not affected by this power pattern. At the edge of the 15′ square field used in the least-squares estimates of the fluctuation levels, the single-dish power pattern is less than 15% of its peak value. We show below that this procedure results in a sensitivity to "sky" fluctuations with an rms value of a factor of 2 or 3 smaller than the actual rms noise level of our maps.

To obtain this sensitivity we must know the radial dependence, if any, of the variance in our maps due to "local" noise. The noise variance is uniform in any map made by taking a direct Fourier transform of a set of visibility data which resulted from uncorrelated noise at each antenna. (See, e.g., Napier and Crane 1982.) The standard VLA procedure (Sramek 1982), first gridding the u-v data with an "exponential-times-sinc" convolution function and then making a map using a discrete Fourier transform, maintains this uniformity to better than 1% within the region closer to the center of a map than to its edge (Greisen 1979). Only this region is "cleaned" and used in our analysis. Therefore, because receiver noise and atmospheric emission at the various dishes are all uncorrelated, they contribute noise uniformly across a map. Also, radio interference is unlikely to produce map features whose amplitude varies systematically with radius, since the result of interference is usually a set of extended stripes across a map (Thompson 1982; Ekers 1982). In conclusion, only the correlator bias and the cross-talk discussed in § III are likely instrumental sources of noise with radially dependent variance. Since the peaks of any such artifacts usually occur well within the primary beam, these effects could lead to an apparent detection of "sky" fluctuations, but they do not invalidate the upper limits we derive below.

a) *Procedure*

Each individual map (which consisted of a square array of square cells each 2″ on a side) was divided into a 32 by 32 array of square blocks, each 64″ on a side (see Figure 1). For each block, we computed the mean value of the intensity (or other Stokes parameter) and the mean square scatter of the intensity about that mean. For each block i, j, we denote this observed mean square scatter by S_{ij}^2. As is usual in an aperture-synthesis map with no strong sources present, the mean values were all close to zero, typically ± 3 μJy. Next, we minimized the sum

$$\sum_{i,j=1}^{14} [S_{ij}^2 - (K^2 + \sigma^2 B_{ij}^2)]^2 , \qquad (1)$$

where K^2 represents the variance of the "local" noise, assumed to be uniform over the map; and σ^2 represents the variance of the "sky" fluctuations, assumed to be uncorrelated with "local" noise, and to be distributed across the map in propor-

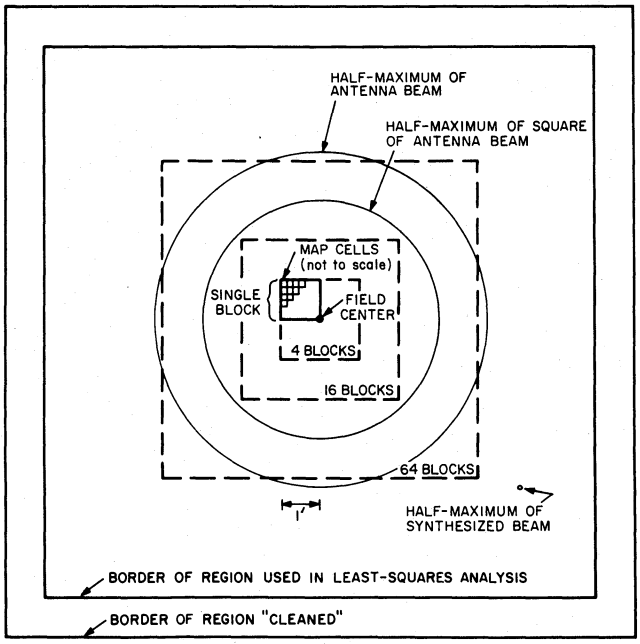

FIG. 1.—Scale diagram of our field of view, showing relative sizes of various regions discussed in the text. The synthesized beam shown is the beam for maps made with no taper applied to the visibility data. The full area of our synthesis maps is four times that of the area "cleaned."

tion to the coefficients B_{ij}^2, which are the values for the blocks i, j of the square of the power pattern of the individual antennas, corrected for several effects which are discussed below. In performing this least-squares analysis, we used only the "cleaned" region of the map (see § IV*b*). To be prudent, we further excluded all blocks at the edges of the "cleaned" region because any noise or errors introduced by the "clean" algorithm are expected to be largest at these edges. Thus we used the central 14 by 14 blocks of our maps (a region 15′ by 15′ in area) as shown in Figure 1. Finally, we also tried to exclude any "wild points" among the S_{ij} values which might have been the result of some unrecognized problem with our maps. To this end we excluded from the final least-squares analysis of each map any S_{ij} values (never more than two, in fact) whose postfit residuals exceeded 3 times the estimated standard deviation of the S_{ij} values (see § V*d*).

b) Calculation of B_{ij}^2

To utilize expression (1), we must calculate B_{ij}^2 for each block. The required coefficients B_{ij}^2 are samples of the square of a symmetric function $B(r)$, where r is the angular distance from the center of the field. This function is the product of the power pattern of the individual antennas and a small correction, itself consisting of two factors. The first factor accounts for the reduction in the variance of the "sky" noise toward the edge of the maps due to the bandwidth used in obtaining the visibility samples, and the second accounts for a similar reduction due to the integration time used in obtaining these samples. As the bandwidth or the integration time increases, the apparent spatial extent of any source not at the phase center of the resulting map increases (e.g., Fomalont and Wright 1974; Perley 1981). Our 55 MHz bandwidth results in a radial "smearing" of the image of an off-center source, and our 30 s integration period causes rotational "smearing." Although the received flux density from each source is nearly conserved, the variance of the resulting map will be decreased. Since we find that the correction is small, we represent it with a simple analytic expression which we obtain by approximating the bandpass, the integration window, the synthesized beam, and the source structure, if any, as Gaussians for which we specify the FWHM. In this approximation the correction to the square of the single-dish power pattern is:

$$[1 + (\alpha r/\theta_{XB})^2]^{-1/2}[1 + (\Delta\phi r/\theta_{XB})^2]^{-1/2} \qquad (2)$$

where α is the ratio of the bandwidth to the radio frequency, r is the angular distance from the center of the field, $\Delta\phi$ is the rotation of the earth during one integration period, and

$$\theta_{XB} = (\theta_X^2 + \theta_B^2)^{1/2} \qquad (3)$$

is the width of the image of a Gaussian source of width θ_X in a map made with a synthesized beam of width θ_B (cf. Class B, Case 1 of Perley 1981). For $\theta_B = 6''$, $\theta_X = 0$ (point source), and $\alpha = 0.0114$, corresponding to a bandwidth of 55 MHz, we find that, at the half-power point of the beam pattern of the individual antennas ($r = 4'.5$), the first correction factor is 0.89, and that at $r = 9'.0$, this factor is 0.70. For a 30 s integration window, which gives $\Delta\phi = 0.002$, the second factor differs from unity by less than 2%, even at $r = 9'.0$. These results apply to maps of any Stokes parameter.

We have so far implicitly assumed that the "sky" noise variance in any given 64″ square block of a map is caused by sources or fluctuations in the corresponding area of the sky. Although the finite resolution and the extended sidelobe structure of the synthesized beam in a strict sense invalidate this assumption, we will show that the treatment given above is adequate to support our conclusions. First, we note that $\theta_B < 64'' \ll \theta_P$, where θ_P is the FWHM of the power pattern of the individual antennas. As θ_B increases from zero, the response in a map due to "sky" noise is "blurred," and as a result, the radial dependence of the variance of the map is altered. The inner portion of the synthesized beam is approximately Gaussian, and it increases the FWHM of the distribution of variance in the map by a factor of $\sim(1 + \theta_B^2/\theta_P^2)^{-1/2}$. Even for the highly tapered maps with $\theta_B \approx 50''$, the change in the FWHM of $B(r)$ would be smaller than those changes in FWHM which were tested and found to cause no statistically significant changes in our results for σ (see Appendix B). Second, in Appendix A we evaluate numerically the effect of the synthesized beam, including its extended sidelobes, on the distribution of variance caused by point sources or sources with a Gaussian profile. We find that the corresponding changes in the B_{ij}^2 values due to the sidelobes of the synthesized beam would be only a few percent of the peak value of B_{ij}^2 near the center of our field and can be ignored when we compute the B_{ij}^2 values for use in expression (1).

Finally, in practice we compute the values of the coefficients B_{ij}^2 at the center of each block rather than as averages over each block. This approximation creates negligible errors in the coefficients (less than 1% of the peak value).

c) Other Models for B_{ij}^2

In order to test the sensitivity of our results to the calculated values of B_{ij}^2, we also used in expression (1) the following analytic forms for $B(r)$, where r is, as before, the distance from the map center:

$$B(r) = 1 - r/10'' \quad \text{(triangle)}, \qquad (4a)$$

$$B(r) = [1 + (r/4')^2]^{-1} \quad \text{(Lorentzian)}. \qquad (4b)$$

These results are discussed briefly in Appendix B.

d) Estimation of the Statistical Errors in K and σ

Our estimates of the statistical errors in the calculated quantities K (instrument and atmospheric noise) and σ (background fluctuation and undetected sources) are based on the assumptions that the values of the quantity S_{ij}^2 in expression (1) are independent samples and that the values of B_{ij}^2 are exact. We assume also that the variance of all S_{ij}^2 are the same—a quantity we will write as VAR$[S^2]$. Then the variances in σ^2 and K^2 are given by

$$\mathrm{VAR}[\sigma^2] = \mathrm{VAR}[S^2] \sum_{i,j} \left(\frac{\partial \sigma^2}{\partial S_{ij}}\right)^2 , \quad (5a)$$

$$\mathrm{VAR}[K^2] = \mathrm{VAR}[S^2] \sum_{i,j} \left(\frac{\partial K^2}{\partial S_{ij}}\right)^2 . \quad (5b)$$

The weighting factors in these equations may be shown, with our assumptions, to be:

$$\sum_{i,j} \left(\frac{\partial \sigma^2}{\partial S_{ij}}\right) = \left[\sum_{i,j} B_{ij}^4 - \frac{1}{N}\left(\sum_{i,j} B_{ij}^2\right)^2\right]^{-1} , \quad (6a)$$

$$\sum_{i,j} \left(\frac{\partial K^2}{\partial S_{ij}}\right) = \left[\sum_{i,j} B_{ij}^4\right] \Big/ \left[N \sum_{i,j} B_{ij}^4 - \left(\sum_{i,j} B_{ij}^2\right)^2\right] . \quad (6b)$$

where N is the number of blocks, generally $(14)^2 = 196$.

To calculate numerical values for VAR$[\sigma^2]$ and VAR$[K^2]$, we need to estimate VAR$[S^2]$. For this purpose, we use the mean square of the postfit residuals, corrected for the number of free parameters:

$$\mathrm{VAR}[S^2] \approx \frac{1}{N-2} \sum_{i,j} [S_{ij}^2 - (K^2 + \sigma^2 B_{ij}^2)]^2 . \quad (7)$$

Equations (5), (6), and (7) were used to find the quantities VAR$[\sigma^2]$ and VAR$[K^2]$; from these, standard deviations of the estimates of σ and K were approximated as $(\mathrm{VAR}[\sigma^2])^{1/2}/2\sigma$ and $(\mathrm{VAR}[K^2])^{1/2}/2K$, respectively. These are the errors we present. Small changes in the estimate of K tend to be accompanied by much larger changes in σ because σ^2 is essentially the quadrature difference between S_{ij}^2 and K^2, and in all cases $\sigma^2 \ll K^2$.

VI. RESULTS

We present first the results from the least-squares analysis of maps made at full resolution, and then some from the analysis of tapered and other, nonstandard, maps.

a) Untapered Maps

The values for K and σ obtained from the least-squares analysis for the total intensity map, and for maps in Stokes parameters Q and V are displayed in Table 1. Note the very weak dependence of the results on the values assumed for θ_{XB}, which enters into the correction factors for B_{ij}^2 (expression [2]). To give some indication of the adequacy of this procedure, we compare in Figure 2 the results from the least-squares analysis with averages of S_{ij}^2, each taken over the set of all blocks at a given distance from the center of the map. This comparison shows that even though the estimate for σ is not statistically consistent with zero, the data do not contain unambiguous evidence of sky fluctuations.

TABLE 1

RESULTS FOR UNTAPERED MAPS

Polarization	Image Width θ_{XB} (arcsec)	Estimated Parameters σ (μJy)	K (μJy)
I	4	5.73 ± 1.24	15.54 ± 0.134
I	6	5.79 ± 1.19	15.52 ± 0.137
I	8	5.82 ± 1.18	15.51 ± 0.138
I	10	5.84 ± 1.17	15.51 ± 0.138
I	12	5.85 ± 1.16	15.51 ± 0.139
Q	6	4.82 ± 0.81	15.24 ± 0.078
Q	12	4.77 ± 0.81	15.23 ± 0.080
V	6	3.94 ± 1.01	14.89 ± 0.081
V	12	3.90 ± 1.00	14.89 ± 0.083

NOTE.—All results here are for $\theta_P = 9'.0$. The estimated parameters and their statistical standard deviations are presented with sufficient figures to reveal the very slight dependence on the value used for θ_{XB}.

b) Tapered Maps

Table 2 shows the results for K and σ obtained with a range of Gaussian tapers applied to the data. In this analysis, we took account of the increase in the width of the synthesized beam θ_B, and also in the resulting image width θ_{XB} which appears in the correction factors in expression (2).

c) Discussion

For all our maps made without taper, $K \gtrsim 3\sigma$, suggesting that instrumental and atmospheric noise dominated any real sky fluctuation, whether due to fluctuations in the microwave background or to unresolved sources. The near equality of the values of the parameter K obtained from the I, Q, and V maps leads to the same conclusion. Nevertheless, the calculated value of σ is significantly different from zero for the total intensity maps. This result would indicate that real sky fluctuations had been detected if the maps made in Stokes parameters Q and V had not also shown similarly significant nonzero values for σ. Indeed, to take these results at face value would imply that the fluctuations in the background are almost completely

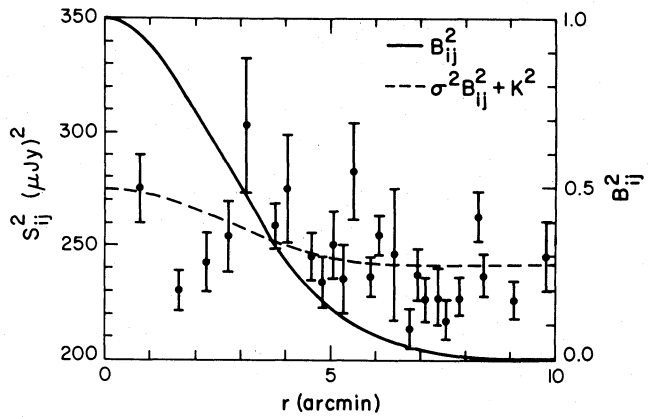

FIG. 2.—Plot of the observed mean square scatter S_{ij}^2 in (μJy)^2 as a function of radial distance from the map center for all values used in the analysis. Each point represents the unweighted mean of all S_{ij}^2 values corresponding to the indicated distance; the vertical bar represents the standard deviation of that mean. The solid line is the square B_{ij}^2 of the effective beam profile (*right-hand ordinate*). The dashed line is the least-squares fit to the observed data points (for $\theta_P = 9'.0$, $\theta_{XB} = 6''$).

TABLE 2

RESULTS FOR TAPERED MAPS[a]

TAPER[b] D_T ($k\lambda$)	SYNTHESIZED BEAMWIDTH θ_B (arcsec)	Ω_B[c] (arcsec)^2	$\mathscr{P}$[d]	ESTIMATED PARAMETERS[e] σ (μJy)	K (μJy)
None	~6	28	1.00	5.8 ± 1.2	15.5 ± 0.1
60	6.5	33	0.89	6.6 ± 1.1	16.9 ± 0.1
25	9.0	59	0.61	7.8 ± 1.6	19.6 ± 0.2
10	14	192	0.26	13.1 ± 2.9	28.6 ± 0.4
5	26	507	0.11	18.2 ± 5.6	38.1 ± 0.8
2.5	51	1143	0.039	32.8 ± 6.5	47.0 ± 1.5

[a] All results here are for total intensity (I) maps and for $\theta_P = 9'.0$ and $\theta_X = 0$.
[b] The radius in the u-v plane at which the Gaussian taper function is 0.3 times its value at the origin.
[c] The effective solid angle of the square of the synthesized beam, as defined by eq. (9).
[d] The total weight of the tapered visibilities relative to the total with no taper (see § VII*b*).
[e] For definitions, see § V*a*.

polarized. In addition, when the total intensity data from our two nights of observation were treated separately, σ was significantly nonzero for *only one* night's data (see Appendix B). Taken together, these results suggest that our values of σ are not the result of true sky fluctuations.

We explored a number of possible causes for these seemingly significant results for σ (see Appendix B). No convincing explanation for excess noise at the map centers, and hence for significant values of σ, emerged from this investigation. Hence we arbitrarily take our estimates of σ, plus twice their estimated standard deviations, as upper limits on the true sky fluctuations. For the total intensity map made without taper, we therefore have 8 μJy as an upper limit on sky fluctuations on scales smaller than the synthesized beam size, $\theta_B \approx 6''$ (see Table 1).

The maps made with taper (Table 2) also show statistically significant nonzero values of σ. Using the same approach here as we used for the maps made without taper, we obtain other upper limits on sky fluctuations. For a taper of 5 $k\lambda$ for which the synthesized beam width is $\sim 26''$, the upper limit is ~ 30 μJy.

These upper limits may be compared to the upper limits found by Fomalont, Kellermann, and Wall (1984) from data obtained with the VLA in the D configuration in which the antennas are more closely spaced. At full resolution ($\theta_B \approx 18''$), they give 17 μJy as an upper limit to the sky fluctuation amplitude; using maps convolved to yield $\theta_B \approx 30''$, they give 39 μJy; and for $\theta_B \approx 60''$, they give 96 μJy.

VII. CONSTRAINTS ON MODEL DISTRIBUTIONS OF SOURCES AND FLUCTUATIONS

We now use the results of the last section to set limits on parameters of models of fluctuations in sky brightness. We do so by calculating for these models the expectation value of σ^2, denoted $\langle\sigma^2\rangle$, and comparing it with our least-squares estimates of σ^2.

a) Unresolved Sources of Equal Flux Density

Let us first consider a simple model of sky brightness in which all the emission comes from a random (Poisson) distribution of unresolved sources each of flux density S_0, where S_0 is below our threshold of ~ 66 μJy for "cleaning." In Appendix A equation (A6) we give an expression for the variance of the map value due to such emission as a function of position in our maps. Because $B(r)$ and $B_{ij}{}^2$ are both normalized to unity at the center of our field, we assume that $\langle\sigma^2\rangle$ is approximately the value of expression (A6) at the center of our field:

$$\langle\sigma^2\rangle = N_0 S_0{}^2 \Omega_B , \tag{8}$$

where N_0 is the mean number of sources per unit area and where Ω_B is defined by

$$\Omega_B = \iint B^2(r) I^2_{\rm beam}(x, y) dx dy , \tag{9}$$

with the origin of the Cartesian x-y coordinate systems being the center of our field, $r = (x^2 + y^2)^{1/2}$ the radial coordinate, and $I_{\rm beam}(x, y)$ the synthesized beam pattern, or "beam map." In computing Ω_B we use the numerical method outlined in Appendix A and we take $B(r) \approx B_P(r)$, the single-dish power pattern, neglecting the small correction factors in expression (2)

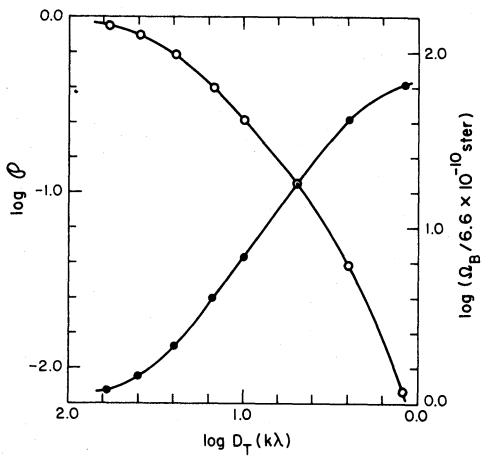

FIG. 3.—The effects of weighting the u-v plane data with a Gaussian taper, as a function of taper width D_T. Open circles (*left-hand ordinate*) represent the ratio $\mathscr{P}$ of the total weight of the tapered visibility data to the total weight of the untapered data. Closed circles (*right-hand ordinate*) represent the ratio of the effective beam area Ω_B to 6.6×10^{-10} sr, the value of Ω_B for an untapered map. See text for definitions. Data points are obtained from computed beam maps; the smooth curves drawn through the points are used in computing the entries in Table 3. The figure shows that Ω_B increases approximately as fast as $\mathscr{P}$ decreases, as the effect of the taper function becomes important.

TABLE 3

UPPER LIMITS ON NUMBER DENSITY OF SOURCES

TAPER D_T ($k\lambda$)	SOURCE FWHM θ_X (arcsec)			
	$\ll 6$	6	12	18
None	0.097	0.13	0.21	0.31
60	0.095	0.12	0.19	0.28
25	0.087	0.10	0.15	0.22
10	0.081	0.087	0.11	0.15
5	0.073	0.075	0.079	0.10

NOTE.—Table entries are upper limits on $N_0 S_0^2$ in sr^{-1} Jy^2 derived from maps made with various tapers.

which depend on the width of the sources. (This definition makes Ω_B an effective solid angle of $I^2_{\rm beam}$, including its sidelobes.) Values of Ω_B for various tapers are included in Table 2 and plotted in Figure 3.

In the last section we took 8 μJy to be the upper limit on the level of "sky" noise in our untapered (full-resolution) map. If $\langle\sigma^2\rangle^{1/2} < 8$ μJy is combined with equation (8), it follows that

$$N_0 < (8 \times 10^{-6})^2 S_0^{-2} \Omega_B^{-1} = 0.097 S_0^{-2} \text{ sr}^{-1} , \quad (10)$$

where S_0 is in janskys, since $\Omega_B \approx 28$ square arcseconds (6.6×10^{-10} sr) for our untapered maps.

We may also use equation (8) to derive limits on N_0 from the tapered maps. The reduced weight of the long-baseline data increases the noise level of the maps and also the least-squares estimate σ and its statistical error. However, taper also results in lower resolution and hence larger Ω_B, and the latter in turn increases the expectation $\langle\sigma^2\rangle$ for any given density N_0. If for each tapered map we take $\langle\sigma^2\rangle^{1/2}$ to be less than the least-squares estimate σ plus twice the statistical error (both given in Table 2), then we obtain the set of limits on $N_0 S_0^2$ which are given in Table 3, in the column for $\theta_X \ll 6''$. As a representative value for the calculations which follow, we take $N_0 S_0^2 < 0.08$ Jy^2 sr^{-1}. We omit results for $D_T = 2.5$ $k\lambda$, because in maps made with this taper the size of the beam is almost that of a block, and the mean square fluctuation within a block is not a good measure of the variance there. Also, for D_T as small as 2.5 $k\lambda$, only the shortest baselines are given full weight and consequently the results may be more subject to systematic errors in the visibility data.

The limits on $N_0 S_0^2$ in Table 3 are comparable with the results of direct source counts down to ~ 200 μJy in this field (Hilldrup, Partridge, and Ratner 1984). The source counts allow $\sim 10^6$ sources per steradian. The limit from our least-squares estimates of σ from the untapered map is weaker: $N_0 < 2 \times 10^6$ sr^{-1} at $S_0 = 200$ μJy. However, the results in Table 3 are significant in that they are valid for arbitrarily small S_0.

b) *Partially Resolved Sources of Equal Flux Density*

In Appendix A we show that the foregoing discussion of the response of the VLA to unresolved sources is easily generalized to apply to models of sky brightness in which emission comes from a Poisson distribution of extended sources, each of total flux density S_0 with an axisymmetric, Gaussian, brightness profile. There we use Fourier transform relations to express the response to Gaussian sources of a map made with a taper function of width D_T (half-width at level 0.3-times-maximum value) in terms of the properties of a beam map formed with a taper function of narrower width D_T' as given by equation (A10). Since the peak response to a source of flux density S_0 in such a map is $S_0 P(D_T')/P(D_T)$, where $P(D_T)$ is the total weight of the visibility data using a taper of width D_T (see Appendix A), equation (8) becomes

$$\begin{aligned}\langle\sigma^2\rangle &= N_0 S_0^2 [P(D_T')/P(D_T)]^2 \Omega_B' \\ &= N_0 S_0^2 [\mathscr{P}(D_T')/\mathscr{P}(D_T)]^2 \Omega_B' , \end{aligned} \quad (11)$$

where $\mathscr{P}(D_T) \equiv P(D_T)/P(\infty)$ is given in Table 2, and where Ω_B' is defined by equation (9) as before, but for a beam map made with a taper of width D_T'. The values of $\mathscr{P}(D_T')$ and Ω_B' can be obtained from Figure 3.

How should we choose D_T to derive a limit on the density on the sky of sources of a given angular size? For the special case of Gaussian sources of FWHM $= \theta_X$ radians, choosing the taper width according to equation (A9) would weight the visibility data in proportion to the visibility amplitude of such sources as a function of radius in the u-v plane. Using a broader taper (larger D_T) would give nearly full weight to visibility samples in which the extended sources are heavily resolved; clearly choosing such a broader taper would reduce our sensitivity to these sources. However, as we saw above in the case of unresolved sources, since the sensitivity of $\langle\sigma^2\rangle$ to N_0 increases with decreasing resolution, there is an advantage in using maps with tapers of narrower width, i.e., smaller values of D_T. Therefore, we use equation (11) to obtain upper limits on $N_0 S_0^2$ from several maps with varying degrees of taper. For each map, we take the estimated value of σ plus twice its standard error (see Table 2) as the limit on $\langle\sigma^2\rangle^{1/2}$. In Table 3 we present upper limits on $N_0 S_0^2$ for sources with Gaussian brightness profiles, and with $\theta_X \ll 6''$ and $\theta_X = 6''$, $12''$, and $18''$. Note the increase in sensitivity to N_0 as narrower taper (smaller D_T) is applied. For instance, the most stringent upper limit on $N_0 S_0^2$ for a random distribution of sources with $\theta_X = 6''$ is actually obtained with a taper $D_T = 5$ $k\lambda$, whereas equation (A9) suggests using $D_T \approx 20$ $k\lambda$ to weight the data in proportion to the expected visibility amplitude.

For sources of angular size $\theta_X \lesssim 12''$, we see that our most stringent upper limits require that the number of sources per steradian be $< 0.08 S_0^{-2}$. For larger sources, for example with $\theta_X = 18''$, the limit is somewhat less stringent, $N_0 < 0.10 S_0^{-2}$. As pointed out for $\theta_X \ll 6''$, these limits on the number of faint discrete sources at 4885 MHz are somewhat weaker than direct counts down to ~ 200 μJy, but are valid for any S_0.

c) *Limits on Temperature Fluctuations in the Microwave Background*

The upper bounds on the quantity $N_0 S_0^2$ may be used to set corresponding limits on the rms fluctuation level of the cosmic microwave background. Limits on this rms temperature fluctuation level, denoted ΔT, depend on the angular size and shape of the fluctuations. For illustrative purposes, we continue to consider the case of fluctuations with Gaussian brightness profiles $T(r)$ parameterized by θ_X and we let the central brightness temperature of each be T_0.

Using the Rayleigh-Jeans law, we find that T_0 and S_0 are related by

$$S_0 = \frac{2kT_0 \Omega_S}{\lambda^2} , \quad (12)$$

where k is Boltzmann's constant, and Ω_S is the effective area of each source, defined by

$$\Omega_S = T_0^{-1} \int 2\pi r T(r) dr \ . \quad (13)$$

For Gaussian sources

$$\Omega_S = \pi \theta_X^2 (4 \ln 2)^{-1} \ , \quad (14)$$

since

$$T(r) = T_0 \exp [-(4 \ln 2) r^2/\theta_X^2] \ . \quad (15)$$

If these sources are Poisson distributed on the sky with a mean density N_0 per steradian, then the expectation value $\langle T^2 \rangle$ of T^2 at any point is

$$\langle T^2 \rangle \approx N_0 \int 2\pi r [T(r)]^2 dr$$
$$\approx N_0 T_0^2 \Omega_S / 2 \ . \quad (16)$$

The factor of 2 arises from the integration because, for Gaussian sources, $[T(r)]^2 = T_0 T(2^{1/2} r)$, as can be seen from the change of variables $r \rightarrow r' = 2^{1/2} r$. Taking the square root of equation (16) and substituting for T_0 from equation (12) yields the rms value ΔT:

$$\Delta T \equiv \langle T^2 \rangle^{1/2}$$
$$= \lambda^2 (2k)^{-1} (2\Omega_S)^{-1/2} N_0^{1/2} S_0 \ . \quad (17)$$

For each value of θ_X, we take the strongest limit on $N_0 S_0^2$ in Table 3 (obtained using eq. [12]) and we use equation (17) to find the corresponding value of the fractional temperature fluctuation level $\Delta T/2.7K$. These results are presented in Table 4, and will be compared with other published limits on the fluctuations of the background in the next section.

TABLE 4

UPPER LIMITS ON TEMPERATURE FLUCTUATION LEVEL

SOURCE FWHM θ_X (arcsec)	$\Delta T/2.7$ K ($\times 10^{-3}$) This Paper	$\Delta T/2.7$ K ($\times 10^{-3}$) Fomalont *et al.* (1984)
6	3.2	...
12	1.7	...
18	1.2	1.0
30	...	0.8
60	...	0.5

NOTE.—Table entries are upper limits on the rms temperature fluctuation, normalized to 2.7 K, due to any randomly distributed Gaussian fluctuations in the microwave background of given FWHM, θ_X. For each value of θ_X, the strongest limit on $N_0 S_0^2$ in Table 3 has been used. In the last column, for comparison, the limits of Fomalont *et al.* (1984) are displayed; note that their upper limits were not calculated in the same manner.

VIII. CONCLUSIONS

The upper limits established here on ΔT are an order of magnitude smaller than the earlier interferometric results of Martin, Partridge, and Rood (1980) on comparable angular scales. Our value for sources of width $\theta = 18''$ is also about an order of magnitude more sensitive than the limits set by Condon and Mitchell (1982) at 21 cm on approximately the same scale, but it is $\sim 20\%$ less sensitive than that established by Fomalont, Kellermann, and Wall (1984). Fomalont *et al.* obtained greater sensitivity to brightness temperature fluctuations primarily because they used the VLA in the more compact D configuration, which gave better coverage of the u-v plane at short baselines. On the other hand, our 8 μJy upper limit on rms sky fluctuation per beam area in our full-resolution map is somewhat lower than their limit at full resolution, either because the systematic errors they discuss were smaller in our C configuration data or because we were more successful in editing our data. Finally, note that for a fair comparison of these various limits the scale size should be identified with some model parameter, such as the width of the fluctuations, θ_X, and not simply with the resolution of the interferometer, θ_B.

Both our results and those of Fomalont *et al.* are adequate to eliminate those models of Hogan (1980) in which $\sim 1\%$ fluctuations in the temperature of microwave background at an angular scale $\sim 10''$ are predicted as a result of the process of galaxy formation at redshifts of order 100. More generally, our limits together with earlier work indicate that the microwave background is isotropic to $\lesssim 0.3\%$ over a wide range of angular scales, extending from $6''$ to $90°$.

Our work could not have been completed without the assistance of NRAO staff members, both at the VLA and in Charlottesville. In particular, we wish to thank John Basart, Bill Cotton, and Kerry Hilldrup. We also thank an anonymous referee for valuable comments on our presentation. At Haverford, this work was supported by NSF grant AST 800737 and to a lesser degree by the Faculty Research Fund of the college; at the Center for Astrophysics, this effort was supported by NSF grant PHY 8243330, the completion of the effort begun at MIT under a predecessor grant.

APPENDIX A

EFFECT OF SIDELOBES OF THE SYNTHESIZED BEAM

In order that the least-squares estimate of σ^2 in expression (1) of § V*a* be a valid estimate of the amount of "sky" noise in a map, the coefficient B_{ij}^2, for each i and j, should be proportional to the sky contribution to S_{ij}^2. If the power pattern of our synthesized beam (hereafter, the beam map) had high sidelobes extending over a region several arcminutes wide, then brightness fluctuations near the center of the field could contribute significantly to values of S_{ij}^2 for blocks throughout that region and not just to values of S_{ij}^2 for blocks near the center. However, in this appendix we show that in our beam maps the sidelobe levels are low enough so that their contribution to S_{ij}^2 can be ignored when the coefficients B_{ij}^2 are calculated. First, we present an analytical expression for the beam map and show how to use it to calculate the expected values of the quantities S_{ij}^2 for "sky" noise from a Poisson distribution of unresolved sources. Then, for our particular set of visibility samples and for each of our choices of taper function, we estimate numerically the contributions to the quantities S_{ij}^2 from "sky" noise which has been scattered through distant sidelobes of the corresponding synthesized beam. Using these esti-

mates, we argue that the contributions from these sidelobes can be ignored when the coefficients B_{ij}^2 are calculated. Finally, we generalize our method to include brightness fluctuations consisting of sources with Gaussian brightness profiles.

In what follows, we may consider that the effects of the single-dish power pattern, and of the finite bandwidth and integration time of the observations, have combined to produce an image of a small region of the sky, and that it is the visibility function of this image which is sampled by the interferometer and transformed to make a map. A VLA synthesis map $I_{\rm map}(x, y)$ may now be expressed in terms of this image, which we denote $I_{\rm true}(x, y)$.

Following Hjellming and Basart (1982), we note that (before any grid correction is made) $I_{\rm map}$ is related to $I_{\rm true}$ by

$$I_{\rm map}(x, y) = \overline{\rm III} * [\bar{C}(\bar{W} * I_{\rm true})] \quad \text{(A1)}$$

and the synthesized beam $I_{\rm beam}(x, y)$ is given by

$$I_{\rm beam}(x, y) = \overline{\rm III} * [\overline{CW}] , \quad \text{(A2)}$$

where the (x, y) dependence of all functions on the right-hand sides is suppressed, an overbar denotes a two-dimensional Fourier transform, and an asterisk denotes a two-dimensional convolution. The function C is the "exponential-times-sinc" convolution function used in the AIPS software package to smooth the visibility data before multiplying by III, which is the sampling (shah) function that consists of a regularly spaced grid of Dirac delta functions in the u-v plane. The function W represents the u-v plane coverage as the sum of another set of delta functions (one for each 30 s average visibility sample), each multiplied by a weighting factor (e.g., to achieve uniform weighting). A radially symmetric taper may be included in these weighting factors; in any case W is normalized so that $I_{\rm beam}(0, 0) = 1$.

If the "sky" noise is due to a Poisson distribution of sources, the variance of $I_{\rm map}$ can be obtained as follows. Consider a uniform partition of the sky into regions of area $dA = dx \cdot dy$ which are so small that $I_{\rm map}$ does not depend on the distribution of the flux density within each region, but only on the total flux density dS of each. According to equation (A1), for any point (x, y), $I_{\rm map}(x, y)$ is a linear function of the image $I_{\rm true}(x', y')$, and we can consider $I_{\rm map}(x, y)$ to be a sum of all the separate responses of $I_{\rm map}(x, y)$ to each region in the partition. For a Poisson distribution, the variance of the number of sources dN in a region of area dA is the same as the mean number of sources, which can be written $N_0\, dA$, where N_0 is the source number density per unit area. If all sources in the sky have flux density S_0, then, as a result of the single-dish power pattern and the other effects mentioned above, the sources in the sky image at a distance r from the center of our field have flux density $S_0\, B(r)$. Therefore, the variance of the flux density in dA is

$$\mathrm{VAR}[dS] = N_0 S_0^2 B^2(r) dA . \quad \text{(A3)}$$

Now let us consider the response $dI_{\rm map}(x, y)$ of $I_{\rm map}(x, y)$ to a given dS. For $dS = 1$ at $r = 0$, that is, for a point source of unit flux density at the center of our field, equations (A1) and (A2) show that $dI_{\rm map} = I_{\rm beam}$ as expected. If dS is offset to $r \neq 0$, the response $dI_{\rm map}$ would be similarly offset, but it would also be altered in shape because of the convolution with the function III. We now show that this effect is negligibly small. The convolution has the effect of adding into map point (x, y) all the values of the function $\bar{C}(\bar{W} * I_{\rm true})$ at all points separated from (x, y) by an integral number of map widths in the x and/or y directions. However, because we use only the inner quarter of each map, these additional, or aliased, contributions all come from points of $\bar{C}(\bar{W} * I_{\rm true})$ which lie more than $1\frac{1}{2}$ map widths ($\sim 50'$) from the center of the field. At these points both $\bar{C}$ and $I_{\rm true}$ are small (the latter due mainly to the single-dish power pattern) and so the effects of aliasing on the variance of $I_{\rm map}$ can be ignored. Thus we may approximate the response $dI_{\rm map}$ for a flux dS at (x', y') as

$$dI_{\rm map}(x, y) \approx I_{\rm beam}(x - x', y - y') dS . \quad \text{(A4)}$$

From this result and using equation (A3) for $r' = (x'^2 + y'^2)^{1/2}$, we obtain

$$\begin{aligned}\mathrm{VAR}[dI_{\rm map}(x, y)] &\approx I_{\rm beam}^2(x - x', y - y')\mathrm{VAR}[dS] \\ &\approx N_0 S_0^2 B^2(r') I_{\rm beam}^2(x - x', y - y') dA . \quad \text{(A5)}\end{aligned}$$

Finally, note that for a Poisson distribution of sources the numbers of sources in any two nonoverlapping regions are statistically independent of each other, and so are the flux densities dS and the responses $dI_{\rm map}(x, y)$. Since $I_{\rm map}(x, y)$ for the entire image $I_{\rm true}(x', y')$ is the sum of all the responses $dI_{\rm map}(x, y)$, the variance $\mathrm{VAR}[I_{\rm map}(x, y)]$ of $I_{\rm map}$ due to the entire image is the sum of all the variances $\mathrm{VAR}[dI_{\rm map}(x, y)]$ from equation (A5). Passing to the limit $dA \to 0$, we obtain an integral expression:

$$\begin{aligned}\mathrm{VAR}[I_{\rm map}(x, y)] \approx N_0 S_0^2 \iint & B^2(r') I_{\rm beam}^2 \\ & \times (x - x', y - y') dx' dy' . \quad \text{(A6)}\end{aligned}$$

This expression allows us to estimate the effect of $I_{\rm beam}$ on our S_{ij}^2 values, and hence on the values required for the coefficients B_{ij}^2.

We seek an upper limit on the effect of the distant sidelobes of $I_{\rm beam}$ on the expectation values $\langle S_{ij}^2 \rangle$. Just as we did for the computation of the S_{ij}^2 from our maps, we divide the beam maps into 64″ square blocks and compute the mean square scatter of $I_{\rm beam}$ in each block. (The difference between the value of this mean square scatter and the value of the mean square of $I_{\rm beam}$ in the same block equals the square of the mean in that block; for $I_{\rm beam}$, as for our "cleaned" maps, this difference is a small fraction of the mean square scatter in most blocks.) To estimate the fractional contribution of all the sidelobes of $I_{\rm beam}$ to the double integral in equation (A6) at an arbitrary point (x, y), we sum the mean square scatters of all the blocks in each of the three nested regions of the beam map shown in Figure 1. [For any map point (x, y) there will be sidelobes of $I_{\rm beam}$ which cause $I_{\rm map}(x, y)$ to respond to "sky" noise from the region of our field of view where $B^2(r') \approx 1$; consequently, to obtain a rough upper limit on the effect of sidelobes, we compute our sums taking $B(r') = 1$ for all r'.] We present results in Table 5 for the beam maps resulting from each of our choices of taper function. These results show that the central $\sim 2'$ by $\sim 2'$ region of $I_{\rm beam}$ contributes much more to the double integral in equation (A6) than does the rest of the $\sim 8'$ by $\sim 8'$ region. In fact, for all the taper functions we use, using the larger region increases the double integral by $\lesssim 10\%$ of the value due to the central $\sim 2'$ by $\sim 2'$ region. These results imply that the amount of variance in any given block due to sources more than $1'$ away is $\lesssim 10\%$ of the variance at the center of our field. This implication in turn permits us to argue that the corrections to the coefficients B_{ij}^2 for the contribution to $\langle S_{ij}^2 \rangle$ of the sidelobes of the synthesized beam would be less than a few

TABLE 5

AREA INTEGRALS OF SQUARE OF SYNTHESIZED BEAM

TAPER D_T ($k\lambda$)	NUMBER OF BLOCKS		
	4	16	64
None	27	28	30
40	39	40	41
15	107	111	120
10	189	196	212
5	503	519	553
2.5	1136	1162	1251

NOTE.—Table entries are in units of square arcseconds and are presented for several taper widths D_T and for integrals limited to regions of the beam containing the indicated number of 64″ square blocks. (See Fig. 1 for schematic definition of the regions and Appendix A for interpretation of the results.)

percent of the values of B_{ij}^2 in the center of the field. In light of the very low sensitivity of our results to changes in $B(r')$ (see § V*c* and Appendix B), we considered it unnecessary to correct our B_{ij}^2 values for the effects of sidelobes.

We now wish to generalize this conclusion to the case of sources with an extended brightness distribution. We show that, just as the effect of sidelobes of the beam map on the expected values of S_{ij}^2 in any map due to a Poisson distribution of point sources can be bounded using the results in Table 5 for the corresponding beam map, so can the effects for a Poisson distribution of extended sources be estimated from the beam maps for more heavily tapered *u-v* data. Consider a source of unit flux density in the center of our field whose brightness profile is denoted $I_{\rm true}$. We compute the image of such a source in a map produced using the weighting W with the help of a beam map made for a new, more heavily tapered weighting W':

$$W' = R\bar{I}_{\rm true} W \,, \tag{A7}$$

where R is the normalization constant required to maintain $I_{\rm beam}(0, 0) = 1$. Application of the Fourier convolution theorem yields the transform

$$\overline{W'} = R\bar{W} * I_{\rm true} \,. \tag{A8}$$

Using this $\overline{W'}$ in equation (A2) shows that the new $I_{\rm beam}$ is R times the image of $I_{\rm true}$, as given by equation (A1), in a map produced using the weighting W. In order to make use of the standard mapping routines, we consider only sources with Gaussian $I_{\rm true}$ and $\theta_X \ll \theta_P$. For such a source, if θ_X is in radians, then $\bar{I}_{\rm true}$ is a Gaussian of FWHM $= (4 \ln 2)/(\pi\theta_X)$ wavelengths, and equation (A7) shows that W' is proportional to the old weighting function W multiplied by an additional Gaussian taper. Following NRAO, we specify the degree of taper by D_T, the radius in the *u-v* plane in wavelengths at which the taper function is 0.3 times its value at the origin. If a map is made with weighting W which includes no taper, the weighting W' given by equation (A7) contains the Gaussian factor $\bar{I}_{\rm true}$, which can be expressed as a taper specified by

$$D_T' = \left(\frac{\ln 0.3}{\ln 0.5}\right)^{1/2} \frac{2 \ln 2}{\pi} \theta_X^{-1}\lambda = 0.582\theta_X^{-1}\lambda \,, \tag{A9}$$

where λ is the wavelength. More generally, if W previously included a taper of width D_T wavelengths, the two Gaussian factors in W' can be combined and expressed as a heavier taper specified by

$$D_T' = [D_T^{-2} + (0.582\theta_X^{-1})^{-2}]^{-1/2}\lambda \,. \tag{A10}$$

To summarize, we have shown that the map response to sources with a Gaussian brightness profile is a constant factor R^{-1} times the response to point sources of a map made with a heavier taper specified by equation (A10). Consequently, for analyzing maps of Gaussian sources as well as of point sources, the results in Table 5 justify neglecting the effects of the sidelobes of our synthesized beam when we calculate the coefficients B_{ij}^2, as long as equation (A10) yields D_T' within the range of the table ($D_T' \gtrsim 2.5k\lambda$).

Finally, for use in § VII*b*, we describe the computation of the constant R. In practice, the weighting function W is not itself normalized to ensure that the peak of the synthesized beam map is unity, but instead, for natural weighting, the weight of each observation is the value of the taper function at the corresponding point in the *u-v* plane. Only later is the sum total of all these weights used to normalize the maps and beam maps. Denoting this total weight by $P(D_T)$ for a map made with taper width D_T, it follows that for a map with this taper $R = P(D_T)/P(D_T')$, where D_T' is obtained from equation (A10) and $P(D_T')$ can be obtained from the plot of $\mathcal{P}(D_T) \equiv P(D_T)/P(\infty)$ in Figure 3. Values of R obtained in this way are used in § VII*b* to compare our least-squares estimates of σ^2 with those predicted for a Poisson distribution of Gaussian sources.

APPENDIX B

ANALYSIS OF NONSTANDARD MAPS

We discuss here our attempts to understand why statistically significant values of σ were found in many of our maps, especially those in Stokes parameters Q and V where none was expected.

First, we analyzed separately the data from each of our two nights of observations. These results and others are collected in Table 6. Note that the value of K, as expected, was $\sim\sqrt{2}$ larger for a single night's data than for the combined data. Although the estimate of σ was significantly different from zero for only one of the I maps, it was significantly different from zero for both Q maps. This result suggests that our values of σ are the result of a time-dependent instrumental problem.

Second, we estimated σ and K from maps constructed with *uniform* weighting of the data in the *u-v* plane. Changing from "natural" weighting to uniform weighting increases the weight of long baselines, and consequently increases the variance of the map due to "local" noise, which is distributed uniformly in the *u-v* plane. The increased noise in the I and Q maps ($K \approx 21.6$ μJy) is clear. The value of σ for the Q map changes little, but the value for the I map becomes insignificant—

TABLE 6

RESULTS FOR NONSTANDARD MAPS[a]

DESCRIPTION OF MAP	POLARIZATION	ESTIMATED PARAMETERS σ (μJy)	K (μJy)
First night only	I	$0.1 \pm \ldots$[b]	22.6 ± 0.12
	Q	6.8 ± 1.3	22.2 ± 0.12
Second night only	I	6.7 ± 1.6	22.9 ± 0.14
	Q	5.9 ± 1.7	22.7 ± 0.14
Uniform weighting	I	1.8 ± 2.4	21.7 ± 0.06
	Q	5.0 ± 0.8	21.5 ± 0.06
No grid correction	I	8.6 ± 0.8	16.0 ± 0.13
13 blocks near discrete sources excluded	I	5.1 ± 0.9	15.3 ± 0.09
	Q	4.5 ± 0.9	15.3 ± 0.08
	V	3.7 ± 1.1	14.9 ± 0.09
Central 4 blocks excluded	I	7.8 ± 1.8	15.6 ± 0.25
	Q	4.5 ± 1.2	16.1 ± 0.09
Central 64 blocks excluded	I	10.3 ± 2.8	15.2 ± 0.14
$\theta_P = 8'$	I	5.5 ± 1.3	15.6 ± 0.13
$\theta_P = 12'$	I	6.2 ± 1.0	15.4 ± 0.17
$B(r) = 1 - r/10'$	I	6.6 ± 1.1	16.3 ± 0.13
$B(r) - [1 + (r/4')^2]^{-1}$	I	6.3 ± 1.1	16.4 ± 0.12
"Instrumental noise map"	I	5.3 ± 4.4	33.0 ± 0.21

[a] All results are for $\theta_{XB} = 6''$ (see text).

[b] Estimate of σ^2 was less than zero; the value shown is $(-\sigma^2)^{-1/2}$.

suggesting again that our values of σ reflect instrumental problems.

Third, to learn whether the "exponential-times-sinc" grid correction (see § IV*a*) might cause excess noise at the center, we analyzed a total intensity map with no grid correction made; σ grew larger, not smaller, as was to be expected if the grid correction had been made properly.

Fourth, we analyzed "uncleaned" maps to see if the "cleaning" process described in § IV*b* could have caused an increase in the estimate of σ. Typically, estimates of σ from "uncleaned" maps differed from those from the corresponding "cleaned" maps by less than one-third of the standard error in σ. The change is small because there were only a few sources detected within our field of view.

Fifth, we examined the residual effect of the identified discrete sources in the maps. Deleting the 13 blocks nearest the sources had little effect on estimates of σ, changing them by less than one standard error (see Tables 1 and 6). As a further check, we analyzed a map in which *only* the "cleaned" discrete sources had been restored, but not the residual background image left after the "clean" procedure terminated. For the total intensity map, we obtained $\sigma = 1.6 \pm 1.2$ μJy. Given such a small value for σ contributed by the sources themselves, we conclude that the sidelobes of the identified discrete sources could have had only a negligible effect on our estimates of σ.

Sixth, we recognized that small biases in correlator outputs or cross-talk between antennas could introduce more noise at the centers of maps than at the edges (§ III). Such effects were found and discussed by Fomalont, Kellermann, and Wall (1984). Although we had edited the data to eliminate just these effects, we nevertheless tried determining σ and K with the central four blocks ($\sim 2'$ by $2'$) and the central 64 blocks ($\sim 8'$ by $8'$) dropped from the map. No significant *decreases* in σ resulted (compare Tables 1 and 6).

Seventh, we estimated σ and K using different values of the width θ_P of the single-dish power pattern to calculate the coefficients $B_{ij}{}^2$ in expression (1), and further tested the sensitivity of our results to the values of $B_{ij}{}^2$ by using two different analytic forms for $B(r)$, as discussed in § IV*c*. The results in Table 6 suggest that only large, unrealistic changes in $B(r)$ would change our results for σ by more than the uncertainties given in Table 1.

Finally, we examined the importance of instrumental problems in the maps by estimating σ and K from an "instrumental noise" map constructed by subtracting a map made with the first night's data from a map made with the second night's. The estimate of K, as expected, increased, but the estimate of σ changed little even though the residuals increased and the resulting statistical error in σ increased to about the same magnitude as σ. Apparently, instrumental effects in some way yielded values of σ as large as those we typically estimated from our maps.

REFERENCES

Bracewell, R. N. 1965, *The Fourier Transform and Its Applications* (New York: McGraw-Hill), p. 249.

Clark, B. G. 1980, *Astr. Ap.*, **89**, 377.

Condon, J. J., and Mitchell, K. J. 1982, *A.J.*, **87**, 1429.

Ekers, R. D. 1982, in *Synthesis Mapping*, ed. A. R. Thompson and L. R. D'Addario (Green Bank, WV: NRAO), chap. 12.

Fixsen, D. F., Cheng, E. S., and Wilkinson, D. T. 1983, *Phys. Rev. Letters*, **50**, 620.

Fomalont, E. B., Kellermann, K. I., and Wall, J. V. 1984, *Ap. J. (Letters)*, **277**, L23.

Fomalont, E. B., and Wright, M. C. H. 1974, in *Galactic and Extragalactic Radio Astronomy*, ed. G. L. Verschuur and K. I. Kellermann (New York: Springer-Verlag), p. 256.

Greisen, E. W. 1979, *VLA Scientific Memorandum No. 131*, NRAO (Charlottesville, VA: NRAO).

Hilldrup, K. C., Partridge, R. B., and Ratner, M. I. 1984, in preparation.

Hjellming, R. M. 1982*a*, in *Synthesis Mapping*, ed. A. R. Thompson and L. R. D'Addario (Green Bank, WV: NRAO), chap. 4.

———. 1982*b*, in *An Introduction to the Very Large Array*, ed. R. M. Hjellming (Socorro, NM: NRAO), chap. 7.

Hjellming, R. M., and Basart, J. P. 1982, in *An Introduction to the Very Large Array*, ed. R. M. Hjellming (Socorro, NM: NRAO), chap. 2.
Hogan, C. J. 1980, *M.N.R.A.S.*, **192**, 891.
———. 1982, *Ap. J.*, **252**, 418; see also Hogan, C. J. 1982, *Ap. J. (Letters)*, **256**, L33.
Kraus. J. D. 1966, *Radio Astronomy* (New York: McGraw-Hill), pp. 159–191.
Lubin, P. M., Epstein, G. L., and Smoot, G. F. 1983, *Phys. Rev. Letters*, **50**, 616.
Martin, H. M., Partridge, R. B., and Rood, R. T. 1980, *Ap. J. (Letters)*, **240**, L79.
Melchiorri, F., Melchiorri, B. O., Ceccarelli, C., and Pietranera, L. 1981, *Ap. J. (Letters)*, **250**, L1.
Napier, P. J., and Crane, P. C. 1982, in *Synthesis Mapping*, ed. A. R. Thompson and L. R. D'Addario (Green Bank, WV: NARO), chap. 3.
Napier, P. J., and Rots, A. H. 1982, *VLA Test Memorandum No. 134* (Socorro, NM: NRAO).
Parijskij, Yu. N., Petrov, Z. E., and Cherkov, L. N. 1977, *Pis'ma Astr. Zh.*, **3**, 483 (English transl. *Soviet Astr.—AJ [Letters]*, **3**, 263).
Partridge, R. B. 1980, *Ap. J.*, **235**, 681.
Perley, R. A. 1981, *VLA Scientific Memorandum No. 138* (Charlottesville, VA: NRAO).
Silk, J. 1968, *Ap. J.*, **151**, 459.
Sramek, R. A. 1982, in *Synthesis Mapping*, ed. A. R. Thompson and L. R. D'Addario (Green Bank, WV: NRAO), chap. 2.
Sunyaev, R. A., and Zel'dovich, Ya. B. 1970, *Ap. Space Sci.*, **6**, 358.
Thompson, A. R. 1982, *IEEE Trans.*, **AP30**, 450.
Uson, J. M., and Wilkinson, D. T. 1984, *Ap. J. (Letters)*, **277**, L1.
Weinberg, S. 1972, *Gravitation and Cosmology* (New York: Wiley), p. 570.
Zel'dovich, Ya. B. 1978, in *IAU Symposium 79, The Large Scale Structure of the Universe*, ed. M. S. Longair and J. Einasto (Dordrecht: Reidel), p. 409.

JAMES E. KNOKE: SofTech, 460 Totten Pond Road, Waltham, MA 02254

R. B. PARTRIDGE: Haverford College, Haverford, PA 19041

MICHAEL I. RATNER and IRWIN I. SHAPIRO: Center for Astrophysics, 60 Garden Street, Cambridge, MA 02138